

Research Article

In silico and in vitro identification of candidate SIRT1 activators from Indonesian medicinal plants compounds database

Azminah Azminah^{a,b}, Linda Erlina^c, Maksum Radji^a, Abdul Mun'im^a, Rezi Riadhi Syahdi^a, Arry Yanuar^{a,*}

^a Faculty of Pharmacy, Universitas Indonesia, Depok, West Java, 16424, Indonesia

^b Faculty of Pharmacy, Universitas Surabaya, Surabaya, East Java, 60284, Indonesia

^c Faculty of Medicine, Universitas Indonesia, Salemba, Jakarta, 10430, Indonesia



ARTICLE INFO

Keywords:

SIRT1 activator
Pharmacophore-based
Virtual screening
Indonesia medicinal plants database (HerbalDB)
Molecular dynamics simulation

ABSTRACT

Sirtuin 1 (SIRT1) is a class III family of protein histone deacetylases involved in NAD^+ -dependent deacetylation reactions. It has been suggested that SIRT1 activators may have a protective role against type 2 diabetes, the aging process, and inflammation. This study aimed to explore and identify medicinal plant compounds from Indonesian Herbal Database (HerbalDB) that might potentially become a candidate for SIRT1 activators through a combination of in silico and in vitro methods. Two pharmacophore models were developed using co-crystallized ligands that allosterically bind with SIRT1 similar to the putative ligands used by SIRT1 activators. Then, these were used for the virtual screening of HerbalDB. The identified compounds were subjected to molecular docking and 50 ns molecular dynamics simulation. Molecular dynamics simulation was analyzed using MM-GB(PB)SA methods. The compounds identified by these methods were tested in an in vitro study using a SIRT-Glo™ luminescence assay. Virtual screening using structure-based pharmacophores predicted that mulberrin as the best candidate SIRT1 activator. Virtual screening using ligand-based pharmacophores predicted that gartanin, quinidine, and quinine to be the best candidates as SIRT1 activators. The molecular docking studies showed the important residues involved were Ile223 and Ile227 at the allosteric region. The MM-GB(PB)SA calculations confirmed that mulberrin, gartanin, quinidine, quinine showed activity at allosteric region and their EC_{50} in vitro values are 2.10; 1.79; 1.71; 1.14 μM , respectively. Based on in silico and in vitro study results, mulberrin, gartanin, quinidine, and quinine had good activity as SIRT1 activators.

1. Introduction

Aging is a systemic process that progressively affects organs and causes dysfunction in cellular homeostasis. It results in a decline in organ function and intervention during physiological trauma (Kitada et al., 2016). Diabetes mellitus is a chronic metabolic disorder that can be caused by various factors, including cell and tissue aging, genetic disposition, obesity, lifestyle factors, and environmental factors, which result in the pancreas not producing adequate insulin, with a consequent elevation in blood glucose concentrations. The prevalence of diabetes increases with age. The International Diabetes Federation reported that, in 2017, there were as many as 10–20 million people with diabetes (www.diabetesatlas.org/across-the-globe.html). Thus, part of the intention behind this study was to identify substances with the capability to slow down the aging process.

Many of targeting signaling pathways play significant roles in

diabetes mellitus, including 5' adenosine monophosphate-activated protein kinase (AMPK), peroxisome proliferator-activated receptor (PPAR) α , β , and γ , histone deacetylases (HDAC), and sirtuin 1 (SIRT1) (Liu et al., 2010). SIRT1 regulates cell metabolism and factors that mediate aging and SIRT1 activator have an impact on treating age-associated diabetes (Dai et al., 2018). Sirtuins are class III members of histone deacetylase (HDAC) family and are involved nicotinamide adenine dinucleotide (NAD^+)-dependent reactions. They are divided into seven types (SIRT1–7) according to the cellular location. Sirtuin improves glucose homeostasis via the $\text{PGC1}\alpha$ complex (Rodgers et al., 2005; Kitada and Koya, 2013), LXR, FXR, AceCS1, UCP2 (Nakagawa and Guarente, 2011), apoptosis, aging, insulin secretion, and regulation (Wanga and Fan Yia, 2012; Pulla et al., 2012; Huynh et al., 2013). In the liver, sirtuin increases gluconeogenesis and reduces glycolysis; it also protects β cells and enhances lipolysis in adipose tissues (www.kegg.jp/kegg/pathway.html). SIRT1 is activated by sirtuin-activating

* Corresponding author.

E-mail address: arry.yanuar@ui.ac.id (A. Yanuar).

<https://doi.org/10.1016/j.compbiolchem.2019.107096>

Received 27 August 2018; Received in revised form 21 June 2019; Accepted 18 July 2019

Available online 18 July 2019

1476-9271/© 2019 The Authors. Published by Elsevier Ltd. This is an open access article under the CC BY-NC-ND license (<http://creativecommons.org/licenses/by-nc-nd/4.0/>).

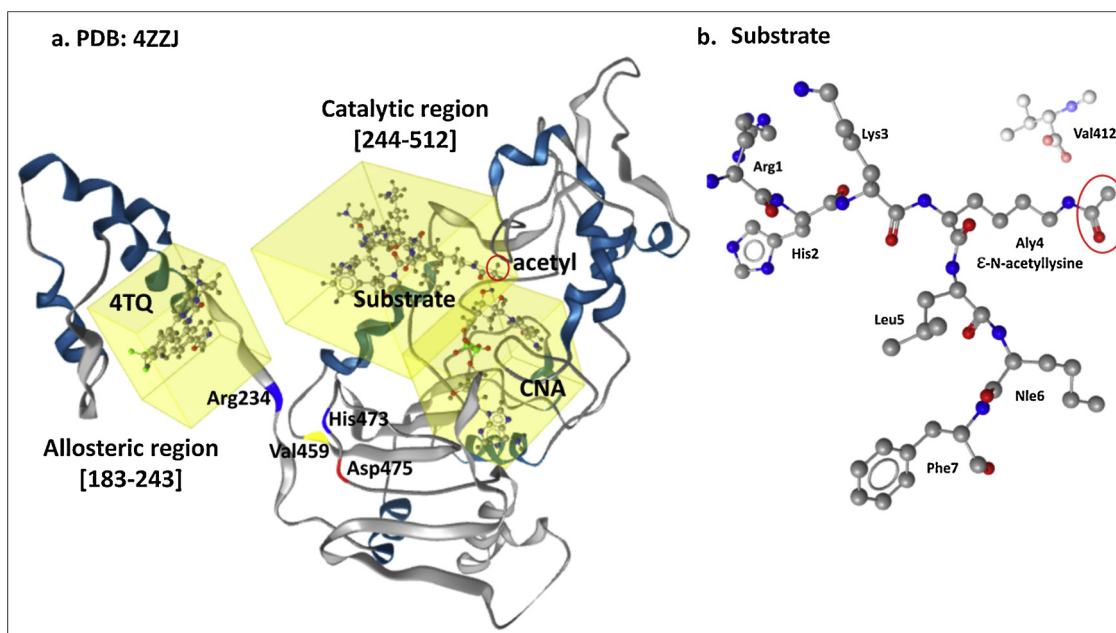


Fig. 1. (a). Crystal structure of human SIRT1 (PDB ID: 4ZZJ), showing allosteric [183–243] and catalytic [244–512] regions and residues involved in important interactions, (b) substrate [Arg1-His2-Lys3-Aly4-Leu5-Nle6-Phe7], visualized using LigandScout 4.2.

compound (STAC), which binds to an allosteric site (Sinclair and Guarente, 2014; Kumar and Chauhan, 2016). Resveratrol is also a sirtuin activator and has been shown to exert anti-aging effects. When combined with metformin, resveratrol improves the quality of metformin therapy for diabetes, indicating that both metformin and resveratrol are antidiabetic agents (Bruckbauer and Zemel, 2013).

This study focused in silico and in vitro on SIRT1 activators. In silico studies allow research on therapeutic substances to be conducted at a relatively low cost through computer modeling such as pharmacophore-based techniques. The pharmacophore-based drug design currently involves two main modeling processes: structure-based and ligand-based pharmacophore processes (Yang, 2010). The present study used both methods, applied to SIRT1 (Protein Data Bank [PDB] ID: 4ZZJ) (Dai et al., 2015). Fig. 1 illustrates the crystal structure of human SIRT1 [PDB] ID: 4ZZJ, showing the allosteric region as STAC-binding domain (SBD) (residues 183–243) [α helix(H)1-turn(T)-H2-T-H3]) and the catalytic region as deacetylase domain [residues 244–512]. The 4ZZJ receptor complex involves important residue interactions, including residue Arg234 at polybasic linker (residues 233–238, Lys-Arg-Lys-Lys-Arg-Lys) from N-terminal STAC-binding domain (SBD) to the catalytic region [Asp475, His473, and Val459] (Fig. 1a). In addition, acetylated p53 (substrate) [Arg1-His2-Lys3-Aly4-Leu5-Nle6-Phe7] (Fig. 1b) interacts as hydrogen bonds of the carbonyl oxygen of Val412 with the ϵ -N of the acetyllysine (substrate/peptide).

The aim of this study was to explore and identify the most potent SIRT1-activating compounds from the Indonesian Medicinal Plants Database (HerbalDB) (Yanuar et al., 2011). The pharmacophores generated from structure-based and ligand-based models were used as templates for virtual screening to select candidate compounds from the HerbalDB. The compound affinity was then confirmed by the molecular docking method. The system was created using molecular dynamics (MD) simulation to examine the constant structural change of macromolecules and substrates at 300 K. As a preliminary MD study, a rigid system was created using AutoDock4Zn to predict the binding affinity of ligand residues. The resulting MD simulation provided values of root mean square deviation and fluctuation (RMSD and RMSF, respectively) and binding affinity through a Molecular Mechanics Generalized Born (Poisson–Boltzmann) Surface Area (MM-GB(PB)SA) calculation (Genheden and Ryde, 2015). The potential for SIRT1 activation was

indicated by activator interactions in the allosteric region, in accordance with the known mechanism for SIRT1 activation (Dai et al., 2010).

The best candidate compounds identified by the in silico study were then subjected to in vitro tests of activity based on a deacetylated enzymatic reaction with SIRT1 and NAD^+ cofactor. The EC_{50} concentration was determined using luminescence intensity data. Finally, the correlation between the in silico and in vitro results was evaluated (Hayes and Archontis, 2011).

2. Materials and methods

2.1. Equipment

The in silico assay used a graphical processing unit with the following specification: operating system, Linux Ubuntu 12.04 LTS 64 bit; processor, Intel® Xeon(R) CPU E5620 @ 2.40 GHz \times 16; and graphics card, NVIDIA Geforce 780 GTX. In addition, a Mac Mini was used with the following specification: operating system OSX Yosemite, version 10.10; a processor, 2.6 GHz Intel Core i5; memory, 8 GB 1600 MHz DDR3; and graphics card, Intel Iris 1536 MB. The in vitro assay used GloMax® Discover software version 3.0 (Madison, WI 53711 USA) with the luminescence mode.

2.2. Protein and compound structures

The three-dimensional (3D) sequence for the human SIRT1 enzyme was obtained from the Protein Data Bank online database PDB ID: 4ZZJ as 4ZZJ.pdb format file (www.rcsb.org/structure/4ZZJ). This was chosen because it included the CNA, peptide (substrate), Zn, in the catalytic region and ligand in the allosteric region. The database for the virtual screening assay used 1377 compounds from the HerbalDB downloaded in the two-dimensional structure with *.smile format (Yanuar et al., 2011).

The active compounds as activators of SIRT1 were collected from previous reports (Kumar and Chauhan, 2016; Mellini et al., 2015; Pulla et al., 2014), including the known active ligand [benzimidazole, imidazothiazole, quinoline, quinazolinone, thiazolopyridine, imidazopyridine, pyrroloquinoline, oxazolopyridine, terpenylated coumarin]

divided into the training set (12 compounds) (Supplementary Fig. 1) and the test set (25 compounds). The 2D structures *.ism file of decoys (1392 compounds) were built using a Directory of Useful Decoys (DUDE) (<http://dude.docking.org/generate>) (Mysinger et al., 2012).

2.3. Pharmacophore model generation and validation

The 3D ligand-based pharmacophores were generated using LigandScout4.2 (Wolber and Langer, 2005). The generation and refinement of pharmacophore models for different SIRT1 activator, therefore, provide a starting point for the design of SIRT1 activator. The pharmacophore models were developed using the LigandScout program.

Structure-based pharmacophore model is built using the 3D pharmacophore-based ligand of the co-crystallized of PDB ID 4ZZJ. Ligand-based pharmacophore model is built from the SIRT1 activators as a training set.

The pharmacophore model from both structure-based and ligand-based were validated using 25 compounds of SIRT1 activator as a test set and 1392 decoys. Various validation parameters were calculated, including sensitivity, specificity, accuracy, receiver operating characteristic (ROC), areas under the curves ($AUC_{1,5,10,100\%}$), and enrichment factors ($EF_{1,5,10,100\%}$) (Bendix et al., 2010).

2.4. Pharmacophore-based virtual screening of HerbalDB compounds

Based on the calculated validation parameters, structure-based and ligand-based pharmacophore models were used for the virtual screening assay. The 1377 plant compounds from the HerbalDB were screened against these pharmacophore models and the hits were scored as the pharmacophore fit score. Lipinski's rule of five from LigandScout and drug-likeness scores and molecular property prediction from Molsoft software (<http://www.molsoft.com>) were applied to select the compounds with the best hits as drug candidates. (Supplementary Fig. 2) shows workflow pharmacophore-based virtual screening of HerbalDB compounds.

2.5. Molecular docking of SIRT1 activator

Molecular docking was performed using AutoDock4Zn (autodock.scripps.edu/resources/autodockzn-forcefield). The compounds selected by the virtual screening were docked with SIRT1 protein (PDB ID: 4ZZJ). Ligands and water molecules were removed to form 4ZZJ [ligand:Zn:carba-NAD:peptide]. Carba-NAD was processed by removing NAD^+ [carba-NAD \rightarrow NAD $^+$].

The parameters of docking were set as follows: grid box npts, $60 \times 60 \times 60$ Å points; grid center, (-0.827; 45.618; -1.076), and a grid-point spacing of 0.375 Å. The number of independent docking runs performed for each docking simulation was set to 100 with 2,500,000 energy evaluations for each run. The structure of the complex was generated as a mesh surface image and interaction by using LigandScout 4.09.1. (Inte: Ligand, Austria)

2.6. Molecular dynamics simulation of SIRT1 activator

The compounds from the database screening with the best affinity were chosen for docking [ligand:NAD $^+$:peptide:Zn:4ZZJ] and MD simulation (Case et al., 2014). The simulation was carried out on Amber Molecular Dynamics using pmemd.cuda in the graphical processing unit environment. The separation of the [ligand:peptide:Zn:NAD $^+$:4ZZJ] complex to be used in the MD simulation then generated the topology and coordinates for ligands, NAD $^+$, Zn, macromolecules, and ligand-macromolecular complexes in a vacuum atmosphere and in water solvents. The AM1-BCC charge was added to the ligand in Antechamber and parameterized by using Sander (Wang et al., 2004; Lee and Duan, 2004). Generating parameters and coordinates of

macromolecule files containing Zn, znb.lib, frmod.zinc, and leaprc-zinc were developed by Pang Lab (mayoresearch.mayo.edu/mayo/research/camdl/zinc_protein.cfm). The original sequence of [Arg1-His2-Lys3-Aly4-Leu5-Nle6-Phe7] substrate was processed by removing Aly with Lys (deacetylation) and Nle with methionine. Thus, The parameters and coordinates of the macromolecules containing the peptide = sequence {NArg His Lys Lys Leu Met CPhe} using tleap and leaprc.ff99SB were developed. Preparations for the formation of NAD $^+$ as a cofactor with a positive charge. To create macromolecules that included NAD $^+$, the parameters of the NAD $^+$.lib and NAD $^+$.frmod files were obtained from Ross Walker (Walker et al., 2002; Pavelites et al., 1996) and the coordinates were changed with those of the NAD $^+$ file bound to the macromolecules. Antechamber was used to add charge to the ligand. During the preparation for the MD simulation, the charge of the system was neutralized by adding Na $^+$ ions. The system was solvated using the water model TIP3BOX octahedron with a size of 12.0 Å. The next process was to run MD simulation for the [ligand:peptide:Zn:NAD $^+$:4ZZJ] complex to obtain an equilibrated system. The solvated [ligand:peptide:Zn:NAD $^+$:4ZZJ] complex by performing a short minimization to ensure the stability of the system with 50 ps of heating and 50 ps of density equilibration with weak restraints on the complex, followed by 500 ps of constant pressure equilibration. The simulation was conducted at 300 K, the default temperature for MD simulations. All simulations were run with SHAKE on hydrogen atoms, a 2-fs time step, and Langevin dynamics for temperature control. The production simulation was run for 50 ns, recording the coordinates every 10 ps. The system dynamics were analyzed for 50 ns and visualized by Visual Molecular Dynamics (VMD). The hydrogen bond interaction limit was set to < 3 Å and the bonding angle to 60°. The resulting MD simulation provided values of RMSD, RMSF, and the binding affinity through MM-GB(PB)SA calculations as implemented in the AMBER package (amber.org). The MM-GBSA and MM-PBSA method is to calculate the free energy difference between two states.

The MM-GBSA, binding free energy to calculate of energy component: VDWAALS (van der walls), EEL (electrostatic interaction), EGB (polar contribution to solvation energy by GB method), ESURF (non-polar contribution to solvation energy using SASA (solvent accessible surface area) for GB.) The MM-PBSA, binding free energy to calculate of energy component (VDWAALS, EEL, EPB (polar contribution to solvation energy by PB method, ENPOLAR (nonpolar contribution to solvation energy from repulsive solute-solvent interactions for PB). The binding free energy delta-G binding, solvated can be calculated, shown in Eq. (1). (Miller et al., 2012). Then, the 2D interaction was visualized snapshot MD using LigandScout 4.09.1.

$$\Delta G_{\text{binding,solvated}} = \Delta G_{\text{complex,solvated}} - (\Delta G_{\text{ligand,solvated}} + \Delta G_{\text{receptor,solvated}}) \quad (1)$$

2.7. In vitro study of SIRT1 activators

The most promising candidate compounds in the in silico study were included in an in vitro study utilizing Promega implemented with SIRT-Glo™ (G6451) (substrate, developer, nicotinamide) (www.promega.com) and SIRT1 active enzymes (S35-31H-05). Quinine and quinidine were obtained from LIPI and PT SIL (Sinkona Indonesia Lestari). Gartanin and mulberrin were purchased from ChemFaces CAS No.33390-42-0, ChemFaces CAS No.62949-79-5, respectively. Determining linear range using SIRT1 enzymes. Prepare serial twofold initial dilution of the SIRT1 active enzymes at 1–5 µg/mL in SIRT-Glo™ Buffer in raws A–D of a white-walled 96-well plate. The final volume of a dilute enzyme in each well should be 100 µl for 96-well plates. Equilibrate 10 ml of SIRT-Glo™ Buffer to the SIRT-Glo™ substrate. Add 10 µl of developer reagent to form the SIRT-Glo™ to form the SIRT-Glo™ Reagent, then mix. Add an equal volume of SIRT-Glo™ SIRT-Glo™ to each assay 100 µM for 96-well. Mix briefly at room temperature using

an orbital shaker at 500–700 rpm to ensure state of being homogeneous. Incubate at room temperature for 15–45 min. Measure luminescence at signal-state. Determining SIRT activator/inhibitor potency, Prepare serial twofold of hit compound and nicotinamide in SIRT-Glo™ buffer in a white-walled 96-well plate. The final volume in each well should be 50 µl for 96-well plates.

Dilute the SIRT enzyme using SIRT-Glo™ buffer to the desired concentration is within the linear range determined. Dispense 50 µl of SIRT-Glo™ enzyme to each well of activator prepared and no-activator controls columns. Add 50 µM of SIRT-Glo™ buffer to the no-sirtuin controls (columns). Mix briefly at room temperature using an orbital shaker at 500–700 rpm to ensure homogeneity and incubate sirtuin/activator mixes at room temperature for at least 30 min. Add an equal volume of SIRT-Glo™ reagent to each assay 100 µl 96-well. Mix and measure luminescence at signal steady-state (15–45 min after adding the SIRT-Glo™ reagent).

The luminescence signal data from the lysine deacetylation reaction on the substrate was used to measure the % activator (EC_{50}). EC_{50} value determined using the aid of GraphPad Prism® software.

3. Results and discussion

3.1. Pharmacophore models and virtual screening

3.1.1. Structure-based pharmacophore model

Structure-based pharmacophore model using the LigandScout program, the 3D pharmacophore-based ligand of the 4TQ ligand of 4ZZJ showed four hydrophobic interactions (HI1, HI2, HI3, and HI4) and one hydrogen bond acceptor (HBA) (Fig. 2).

The calculated validation parameters for the 3D-pharmacophore model of SIRT1 (4ZZJ) (Fig. 2c) generated using LigandScout 4.09.1 were as follows: $AUC_{1,5,10,100\%}$, 0.78, 0.95, 0.97, and 0.57, respectively; $EF_{1,5,10,100\%}$, 12.1; 4.0; 3.5; and 3.5, respectively; accuracy, 93%; and specificity, 94%. These values complied with the requirements for $AUC_{1,5,10,100\%}$ all to be > 0.5 and $EF_{1,5,10,100\%}$, all to be > 1. The virtual screening produced 81 hits out of the 25 active compounds and 1392 decoys.

The virtual screening against HerbalDB compounds captured as hits the compounds that showed the spatial overlap of their chemical group (map) with corresponding features in the pharmacophore model. The total number of molecules were obtained after searching the website <http://herbaldb.farmasi.ui.ac.id>. Ten compounds showed the highest pharmacophore fit scores (Supplementary Table 1) and were tested using Molsoft software (<http://www.molsoft.com>) to investigate their drug-likeness scores and molecular property prediction. Lipinski's rule was also applied as the main standard to identify the compounds that were the most likely drug candidates. The evaluation of drug-likeness involved assessing whether the parameters in Lipinski's rule of five

were met, that is, molecular weight < 500 g/mol, < 10 HBAs, < 5 hydrogen bond donors (HBDs), and a partition coefficient clogP value < 5 (Lipinski, 2004).

Based on the drug-likeness score and the molecular property prediction, the best hit among the 10 compounds was mulberrin. Mulberrin ($C_{25}H_{26}O_6$) 2-(2,4-dihydroxyphenyl)-5,7-dihydroxy-3,8-bis(3-methylbut-2-enyl)chromen-4-one (Mr: 422.477 g/mol) has five HBAs, four HBDs, six (Methylbut-2-enyl and phenyl group) as hydrophobic interactions (HI), 3 aromatic rings (AR), cLogP = 5.3, and a drug-likeness score of 1.17 (Supplementary Fig. 3).

Mulberrin has similar structure chromen-4-one group of SIRT1 activator (7-hydroxy-4H-chromen-4-one) (Kumar and Chauhan, 2016). Mulberrin compounds are found in the plants *Artocarpus heterophyllus* and *Morus australis*. Mulberrin has been shown to reduce the type 2 diabetes in mice significantly (Wilson and Islam, 2015).

3.1.2. Ligand-based pharmacophore model

Modeling 3D-pharmacophore ligand-based active compounds of SIRT1 as training sets were used for virtual screening with LigandScout4.09.1. This resulted in ten 3D-pharmacophore models (Supplementary Table 2). Of these, Model 1 had the highest score of 0.7729; its features comprised two hydrophobic interactions (HI1 and HI2), two aromatic rings (AR1 and AR2), and HBA. Fig. 3 shows the calculation of the distance between the pharmacophore features for Model 1.

The validation of ligand-based 3D pharmacophore models was performed automatically using the LigandScout program, calculating $EF_{1\%}$ values and AUC based on ROC curves (which should be > 0.5) (Table 1).

The evaluation results for Models 1 to 10 given in Table 1 showed that Model 1 was the best, with an AUC value of 0.88 and sensitivity of 0.84%, specificity of 0.91%, accuracy of 91.1%; this was therefore chosen for the pharmacophore model for SIRT1 activator virtual screening. The screening of 1377 compounds from HerbalDB resulted in 18 compounds with the features HI1, HI2, AR1, AR2, and HBA (Supplementary Table 3). The compounds with the highest Pharmacophore-Fit Score were quinine (54.11), quinidine (53.46), and gartanin (53.42), indicating they were the best candidate SIRT1 activators. Then, these compounds were screened with Lipinski's rules and by using the Molsoft drug-likeness program. The results for the three compounds were as follows (Supplementary Figs. 4–6). Quinine ($C_{20}H_{24}N_2O_2$), (R)-[(2S,4S,5R)-5-ethenyl-1-azabicyclo[2.2.2]octan-2-yl](6-methoxyquinolin-4-yl)methanol (Mr: 324.424 g/mol) has three HBAs, one HBD, three (ethenyl and quinolinyl group) as hydrophobic interactions, 2 aromatic rings (AR), cLogP = 2.887, and a drug-likeness score of 0.88. Quinine compounds cause hypoglycemia in malaria sufferers (Ogetii et al., 2010).

Quinidine ($C_{20}H_{24}N_2O_2$) (S)-[(2R,4S,5R)-5-ethenyl-1-azabicyclo

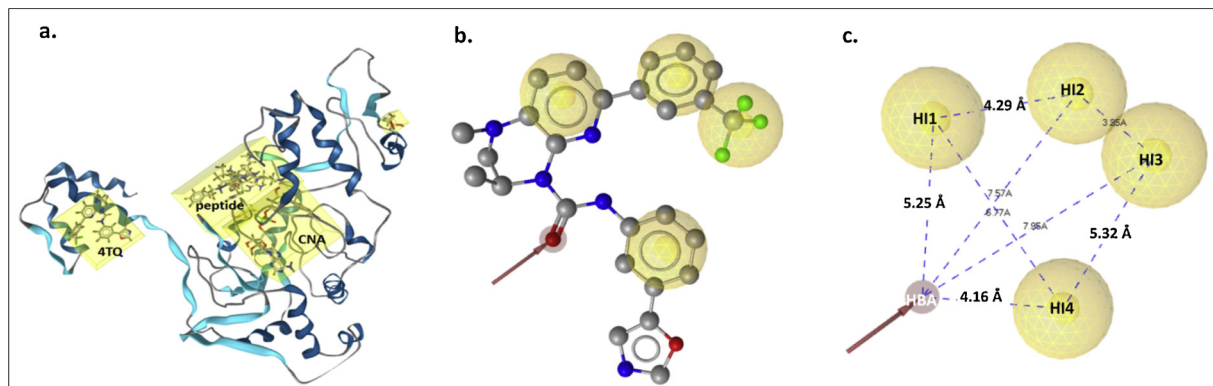


Fig. 2. Pharmacophore building of the SIRT1 ligand using the LigandScout program. (a) SIRT1. (b) The 3D pharmacophore. (c) Pharmacophore features of the co-crystallized 4TQ Ligand. HI1, HI2, HI3, and HI4: hydrophobic interactions; HBA, hydrogen bond acceptor.

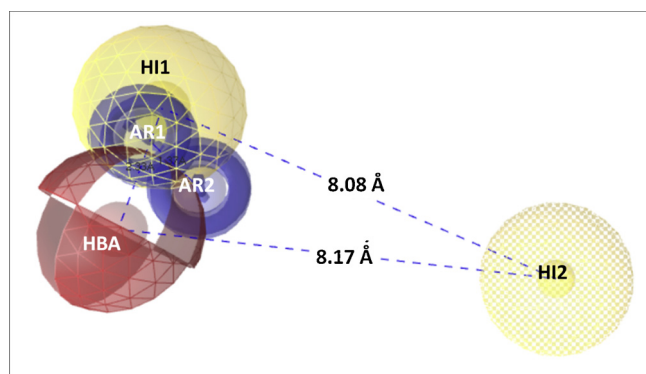


Fig. 3. Pharmacophore Model 1, showing some of its features and the distances between them. HI1 and HI2, hydrophobic interactions; AR1 and AR2, aromatic rings; HBA, hydrogen bond acceptor.

Table 1

Areas under curve (AUC) and enrichment factors (EF) for Models 1–10 obtained from the ligand-based virtual screening validation.

Model	AUC 100%	EF 1%	Sensitivity%	Specificity%	Accuracy %
1	0.88	12.1	0.84	0.91	91.1
2	0.86	8.1	0.80	0.91	90.8
3	0.84	12.1	0.92	0.63	63
4	0.90	16.2	0.96	0.60	61
5	0.76	0.0	0.96	0.47	48
6	0.88	16.2	0.96	0.58	58
7	0.90	16.2	1.00	0.44	45
8	0.78	20.2	0.92	0.62	60
9	0.79	16.2	0.92	0.62	65
10	0.92	12.1	1.00	0.62	46

[2.2]oct-2-yl](6-methoxyquinolin-4-yl)methanol (Mr: 324.424 g/mol) has three HBAs, one HBD, three (ethenyl and quinolinyl group) as hydrophobic interactions, 2 aromatic rings (AR), cLogP = 2.887, and a drug-likeness score of 0.88. Quinidine compounds are found in the *Cinchona calisaya* plant and have been used for malaria drugs. There is a relationship between quinidine compounds and insulin secretion (Phillips et al., 1986; medlineplus.gov/ency/article/000310.htm). Quinine and Quinidine have similar structure with quinolines group of SIRT1 activator (Vu et al., 2014).

Gartanin (C₂₃H₂₄O₆) 1,3,5,8-Tetrahydroxy-2,4-bis(3-methylbut-2-en-1-yl)-9H-xanthen-9-one (Mr: 396.439 g/mol) has five HBAs, four HBDs, five hydrophobic interactions (HI), 3 aromatic rings (AR). cLogP = 4.786, and a drug-likeness score of 0.15. Gartanin compound is found in *Garcinia dulcis* and *G. mangostana* (mangosteen) plants and have been used to treat mumps and swellings (Pedraza-chaverri et al., 2008). Gartanin has similar structure to γ -mangostin, a xanthone from mangosteen of SIRT1 activator (Wang et al., 2018). An ethanol extract of *G. mangostana* has been shown to exhibit hypoglycemic activity (Taher et al., 2016).

3.2. Molecular docking

The ligand 4TQ was re-docked using AutoDock4Zn into the macromolecule crystal of PDB: 4ZZJ to evaluate the RMSD. Lower values of RMSD indicate greater similarity between the re-docked compound and the reference. RMSD values < 2.0 Å were considered acceptable. The binding sites for 4TQ with 4ZZJ were at residues Leu206, Pro211, Pro212, Ile223, Ile227, as hydrophobic residues and Thr209, Gln222, Asn226 as hydrophilic residues.

The four screened compounds (mulberrin, quinine, quinidine, and gartanin), resveratrol (C₁₄H₁₂O₃) 5-[2-(4-hydroxyphenyl)ethenyl]benzene-1,3-diol (as a positive control) and nicotinamide (as a negative control) were docked into 4ZZJ at allosteric region (alpha helix(H)1-

turn(T)-H2-T-H3) using AutoDock4Zn to evaluate the binding energy to estimate the ligand's affinity towards the macromolecule.

The molecular docking score of mulberrin showed binding energy of -4.89 kcal/mol (Fig. 4a and b). Essential residues of SIRT formed in the mulberrin:4ZZJ complex included methylbut-2-enyl group contacts with Leu206 and Ile227 as Hydrophobic Interaction (HI), and -OH (hydroxy) group bonding with Ile223, Thr209, and Asn226 as HBD (hydrogen bonding donor).

Quinine had a docking score of -4.71 kcal/mol, with interactions of quinine-4ZZJ at quinolin-4-yl group with residues Leu206 (HI), Ile223, Ile227 (HI) and -OH (hydroxy) group with Ile223 (HBD), (Fig. 4c). Quinidine had a docking score of -4.98 kcal/mol, with interactions of quinidine-4ZZJ at quinolin-4-yl group with residues Thr206 (HI), Ile223 (HI), Ile227 (HI) and ethenyl group with Thr209 (HI) (Fig. 4d). Gartanin had a docking score of -5.67 kcal/mol, with interactions of gartanin-4ZZJ at the methylbutenyl group with residues Leu202, Leu206 (HI), Thr209 (HI), Thr219 (HI), Ile223 (HI), and xanthone group with Ile227 (HI) (Fig. 4e). In comparison, the resveratrol compounds had a docking score of -4.29 kcal/mol, with interactions of resveratrol-4ZZJ at -OH (hydroxy) with hydrophilic residues Gln222 and phenyl-ethenyl group with Thr219, Ile223 as hydrophobic interaction. Nicotinamide had a docking score of -4.63 kcal/mol, with interactions of nicotinamide-4ZZJ at benzene group with residues Ile210 (HI), and -NH₂ group with Pro207 (HBD) (Supplementary Fig. 7) The docking scores for mulberrin, quinine, quinidine, and gartanin were better than that for the resveratrol compounds (active compound of SIRT1).

The results of molecular docking calculations the binding site for 4TQ, mulberrin, quinine, quinidine, gartanin, resveratrol, nicotinamide with 4ZZJ and in the allosteric region are summarized in Fig. 5. In molecular docking studies, the important residues involved were Ile223 and Ile227, which interacted hydrophobically with all four compounds, similar to the crystal ligand in 4ZZJ (Dai et al., 2015), except nicotinamide (as SIRT1 inhibitor) no interaction with Ile223 and Ile227.

3.3. Molecular dynamics simulation

The MD simulations for the [4ZZJ:NAD⁺:Zn:peptide] complex and each of the four compounds, nicotinamide, no ligand (apo) were run for 50 ns at a temperature of 300 K (27 °C). The processes of minimization, equilibration, and production were performed using Amber. The system was first checked at the minimization level to make sure the ligand bound to the protein (the macromolecule). The equilibration state included checking the temperature, pressure, and energy were stable and optimized to make sure the system would continue for 50 ns.

System dynamic stability was determined by the values of RMSD and RMSF. Based on the RMSD of each compound with 4ZZJ:NAD⁺:Zn:peptide (Supplementary Fig. 8) shows the RMSD values and the differences for five conformational changes (flexibility) at allosteric and catalytic region. Interaction ligand:4ZZJ complex stable in the allosteric region of the [4ZZJ:NAD⁺:Zn:peptide] complex during 1–50 ns of the simulation. In the figure, it can be seen that the nicotinamide complex shows interaction only for 10 ns, whereas at 20 ns it does not show interactions between nicotinamide and [4ZZJ:NAD⁺:Zn:peptide].

The RMSFs are shown in Supplementary Fig. 9. The duration of the simulation was set to 50 ns to extend the monitoring of the flexibility and complexity of the macromolecule at the allosteric site. Amino acid residues such as Ile223, Ile227 (hydrophobic) and Asn226, Glu230 (hydrophilic) were the key to the allosteric sites of the ligands of mulberrin, quinine, quinidine, or gartanin with [4ZZJ:NAD⁺:Zn:peptide]. At these residues, the RMSF was relatively low, indicating that the compounds (mulberrin, quinine, quinidine, or gartanin) had bound to the receptor (allosteric region).

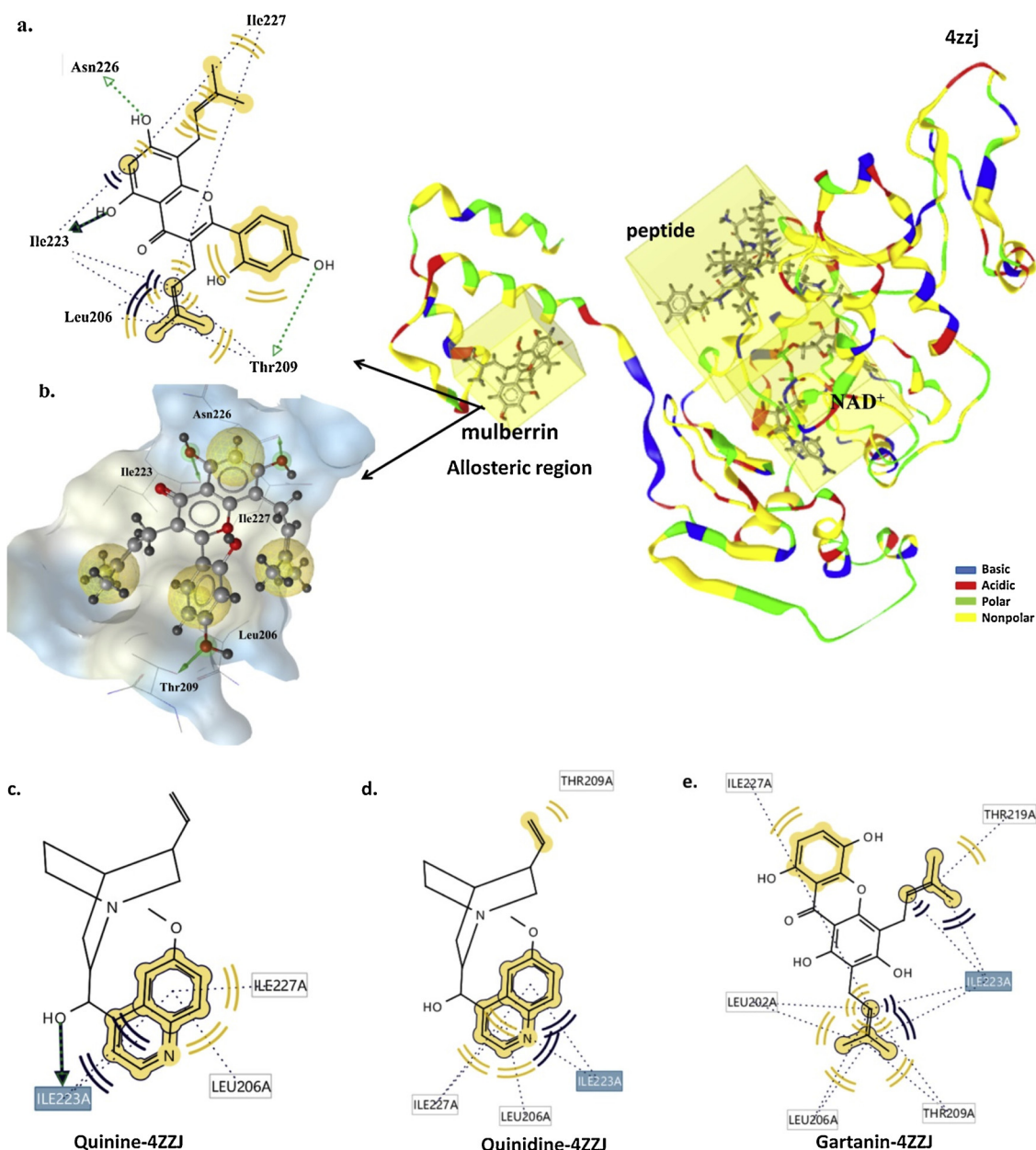


Fig. 4. (a) Two-dimensional scheme of the interaction between mulberrin and the 4ZZJ complex, generated by LigandScout 4.2. (b) The structure of mulberrin and 4ZZJ complex shown as a mesh surface image, generated by LigandScout (hydrophilic, blue; hydrophobic, grey). The interaction between (c) quinine, (d) quinidine, (e) gartanin, with the 4ZZJ.

3.4. Hydrogen bond interaction

The hydrogen bond occupancy can be divided into three categories: weak (25%–50%), strong (50%–75%), and very strong (75%–100%) (Kästner et al., 2009). The 10 ns MD simulation of SIRT1 with the compounds reveal the hydrogen bond occupancy between allosteric region residue (Arg234) and catalytic region residues (Asp475, His473 and Val459) is shown at Fig. 6.

The 4ZZJ complex with SIRT1 activator involves important residue interactions, including guanidinium group interaction between Arg234 via hydrogen bond formation [NH-O] with Asp475. The hydrogen bond interaction [NH-O] was also observed between residues Arg234 with His473 and Val459, which have a key role in enzyme activation (Dai et al., 2015). The interaction between Arg234 and Asp475 via hydrogen bond formation [NH-O] was observed during MD simulation of SIRT1 complex with mulberrin (99.9%); quinine (99.8%); quinidine (99.7%);

gartanin (99.9%); nicotinamide (99.4%); apo-form (99.8%). Thus, the complex of SIRT1 with mulberrin, quinine, quinidine, gartanin, nicotinamide and apo-form showed very strong bond with residue Arg234 (in the allosteric region of SIRT1) to Asp475 (in the catalytic region), indicating their enzyme activity.

The hydrogen bond interaction [NH-O] were observed between NH and carbonyl group of Arg234 and His473 of SIRT1 with mulberrin (26.9%), quinine (10.5%), quinidine (31.3%), and gartanin (12%), nicotinamide (62.7%), apo (53.5%). Nicotinamide and apo form shows more occupancy interactions than the other compounds.

The hydrogen bond interactions were observed between Arg234 and Val459 residues of SIRT1 with mulberrin (75.8%), quinine (71.4%), quinidine (83.8%), gartanin (72.9%), nicotinamide (57.3%), apo-form (62.3%). The complex of SIRT1 with mulberrin, quinine, quinidine and gartanin showed very strong bond, while nicotinamide and apo form of the enzyme show the strong bond with residue Arg234 in the SIRT1

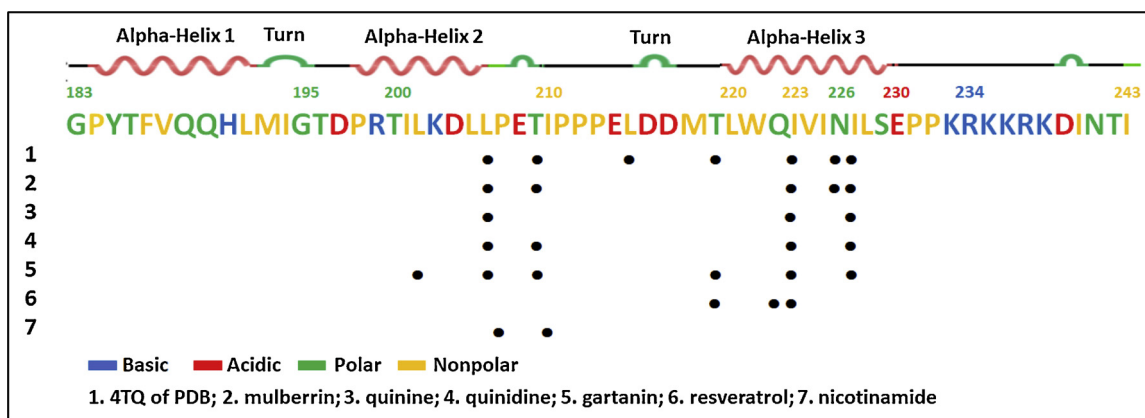


Fig. 5. Interactions between the residues on the SIRT1 allosteric site and the ligands of (1) 4TQ in the crystal structure of 4ZZJ, and the results of the molecular docking of (2) mulberrin, (3) quinine, (4) quinidine, (5) gartanin, (6) resveratrol, (7) nicotinamide.

allosteric region to His473 in the SIRT1 catalytic region.

The hydrogen bonds occupancy of the carbonyl oxygen of Val412 of SIRT1 with the N of the deacetylated-lysine 4 of the peptide substrate was also observed during 10 ns of MD simulation with mulberrin (90.0%); quinine (91.2%); quinidine (96.8%); gartanin (83.9%), and apo-form (80.0%) (Fig. 6). The complex of SIRT1 with mulberrin, quinine, quinidine, gartanin and apo-form showed very strong hydrogen bond occupancy with N atom of the deacetylated-lysine. Nicotinamide as SIRT1 inhibitor was observed to be a weaker bond with 55.8% hydrogen bond occupancy of Val412 with atom N of the deacetylated-lysine.

3.5. Binding free energy calculations for the receptor–ligand interaction

The binding free energy calculated by molecular docking was recalculated using the MM-GB(PB)SA method. The calculation of binding free energy using the molecular mechanics Poisson–Boltzmann (MM-PBSA) and generalized Born surface area models MM-GBSA, respectively) methods gave more selective results to estimate ligand-binding affinities. (Karaman and Sippl, 2015; Genheden and Ryde, 2015).

These calculations of binding free energy for the interactions of mulberrin, quinine, quinidine, and gartanin ligands with SIRT1 in the allosteric region [α helix(H)1-turn(T)-H2-T-H3] resulted which evaluated on the trajectory at the end of 50 frames of 10, 20, 30, 40, and 50 ns simulation (Table 2).

The binding free energy MM-GBSA calculation according to Miller method resulting the $\Delta G = -17.37 \pm 2.805$ kcal/mol of SIRT1-mulberrin complex. (Supplementary Fig. 10) (Miller et al., 2012).

Mulberrin-SIRT1 complex show interaction methyl butenyl group with Ile223 and methyl butenyl, phenyl group with Ile227 at the allosteric site of the trajectory at the end of 50 frames of 10, 20, 30, 40, and 50 ns simulation (Fig. 7). The minimum binding free energy (MM-GBSA $\Delta G = -27.258 \pm 2.984$ kcal/mol) of mulberrin with 4ZZJ at 20 ns, with interactions of methyl butenyl group with Thr209, Leu215, Ile223, Ile227 as hydrophobic interactions (4 amino acids) and $-OH$ (hydroxyl) group with Asn226 (HBA), Pro470 (HBD). The maximum binding free energy was at 30 ns, with interactions of methyl butenyl group with six amino acids of Leu202, Leu206, Thr209, Ile223, Ile227 as hydrophobic interactions (Table 2, Supplementary Fig. 11). The difference between the maximum and minimum energy (Δ) is

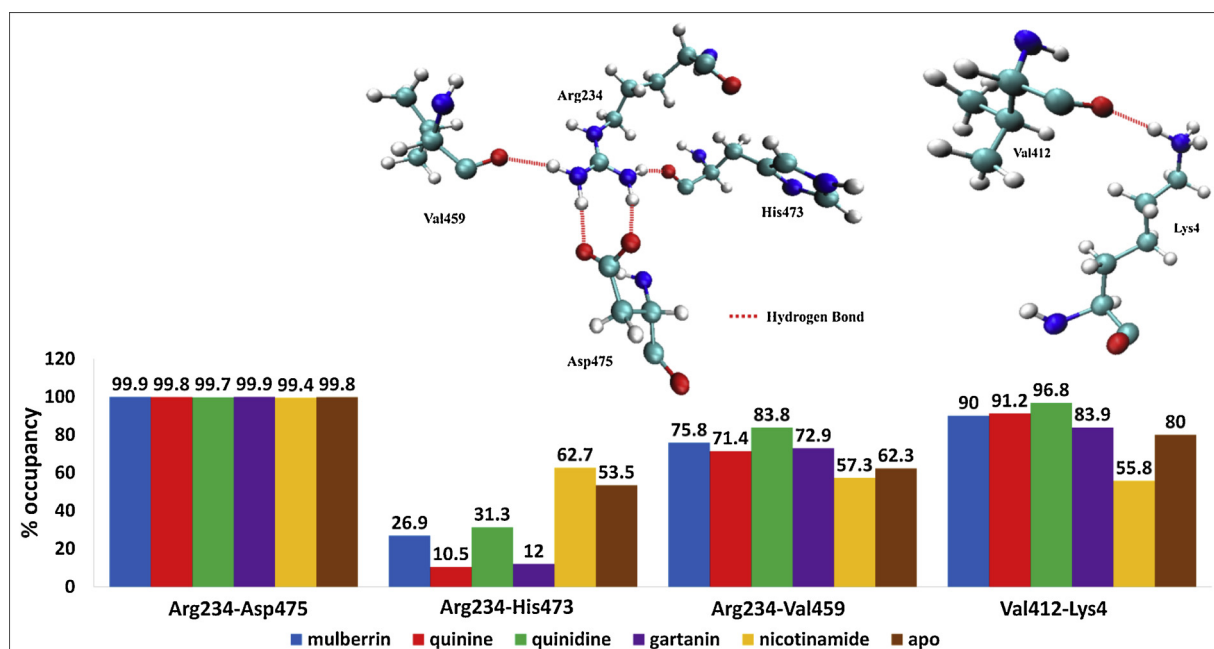


Fig. 6. Hydrogen bond strength (% occupancy) show the important residues of Arg234-Asp475; Arg234-His473; Arg234-Val459; Val412-Lys4 in SIRT1 complex [4ZZJ:NAD + Zn:peptide] obtained from 10 ns MD simulation of SIRT1 with mulberrin, quinine, quinidine, gartanin, nicotinamide, and apo-form.

Table 2

The binding free energy MM-GB(PB)SA of SIRT1 [4ZZJ:NAD⁺:Zn:peptide] complex with the mulberrin, quinine, quinidine, gartanin of the trajectory at the end of 50 frames of 10, 20, 30, 40, and 50 ns simulation.

	10 ns	20 ns	30 ns	40 ns	50 ns
mulberrin	-17.367 ± 2.805 (-17.931 ± 3.056)	-27.258 ± 2.984 (-24.323 ± 3.682)	-10.771 ± 3.744 (-13.047 ± 3.729)	-14.725 ± 1.859 (-16.525 ± 2.182)	-16.420 ± 1.956 (-17.900 ± 2.365)
quinine	-19.259 ± 2.354 (-18.497 ± 2.283)	-18.886 ± 1.850 (-16.922 ± 3.073)	-15.959 ± 2.199 (-15.631 ± 2.209)	-28.455 ± 2.326 (-24.250 ± 2.549)	-27.747 ± 2.823 (-24.125 ± 3.077)
quinidine	-18.274 ± 2.395 (-16.693 ± 2.521)	-17.976 ± 2.806 (-19.380 ± 2.383)	-14.427 ± 3.487 (-15.023 ± 3.780)	-16.736 ± 1.969 (-17.817 ± 2.015)	-17.968 ± 2.000 (-18.911 ± 2.281)
gartanin	-18.593 ± 1.945 (-19.840 ± 2.326)	-18.027 ± 1.820 (-19.403 ± 2.103)	-24.896 ± 2.578 (-22.383 ± 2.564)	-16.932 ± 2.690 (-18.159 ± 2.770)	-19.373 ± 2.458 (-19.769 ± 3.165)

MM-GB(PB)SA results ΔG are reported in kcal/mol. The number in parentheses indicated of MM-PBSA results.

16.487 kcal/mol, this is due to the interaction of the presence of hydroxyl (-OH) with Asn226 as hydrophilic at 20 ns. The minimum binding free energy MM-PBSA ΔG was -24.323 ± 3.682 kcal/mol at 20 ns; the difference with the maximum energy, at 30 ns, was $\Delta = 11.276$ kcal/mol.

Quinine-SIRT1 complex show hydrophobic interaction quinolinyl group and pyridine of quinolinyl group with Ile223 at the allosteric site of the trajectory at the end of 10, 20, 30, 40, and 50 ns simulation (Table 2, Supplementary Fig. 11). Quinine complexed with the SIRT1 showed the minimum binding free energy (MM-GBSA $\Delta G = -28.455 \pm 2.326$ kcal/mol) at 40 ns, with interactions of hydroxyl (-OH) group with Lys233 [HO-N] as hydrophilic interaction and quinolinyl group with Thr219 and Ile223 and ethenyl group with Leu450 (catalytic region) as hydrophobic interaction. The maximum binding free energy was at 30 ns, with interactions of ethenyl group with Ile227, Leu206, quinolinyl group with Leu215, Ile223 as hydrophobic interaction. The difference between the maximum and minimum energy (Δ) = 12.496 kcal/mol. this is due to the interaction of the presence of hydroxyl (-OH) with Lys233 as hydrophilic interaction and Leu450

(catalytic region) as hydrophobic interaction at 40 ns, The minimum binding free energy MM-PBSA ΔG was -24.250 kcal/mol, at 10 ns; the difference with the maximum energy, at 30 ns, was $\Delta = 8.619$ kcal/mol.

Quinidine-SIRT1 complex show interaction of hydroxyl group with Thr209; ethenyl group and benzene of quinolinyl group with Ile223 and ethenyl group with Ile227 at the allosteric site of the trajectory at the end of 50 frames of 10, 20, 30, 40, and 50 ns simulation (Table 2, Supplementary Fig. 11). Quinidine complexed with the SIRT1 showed the minimum binding free energy MM-GBSA $\Delta G = -18.274 \pm 2.395$ kcal/mol at 10 ns, interactions with hydroxyl of quinidine with Thr209 [OH-O], ethenyl group with Ile223, Ile227 as hydrophobic interaction. The maximum binding free energy was at 30 ns, with interactions ethenyl group with Ile227, quinolinyl group with Ile227; The difference between the maximum and minimum energy $\Delta = 3.84$ kcal/mol within the standard error of MM-GBSA binding energy. The minimum binding free energy MM-PBSA ΔG was -19.38 kcal/mol, at 20 ns; the difference with the maximum energy, at 30 ns, was $\Delta = 2.68$ kcal/mol.

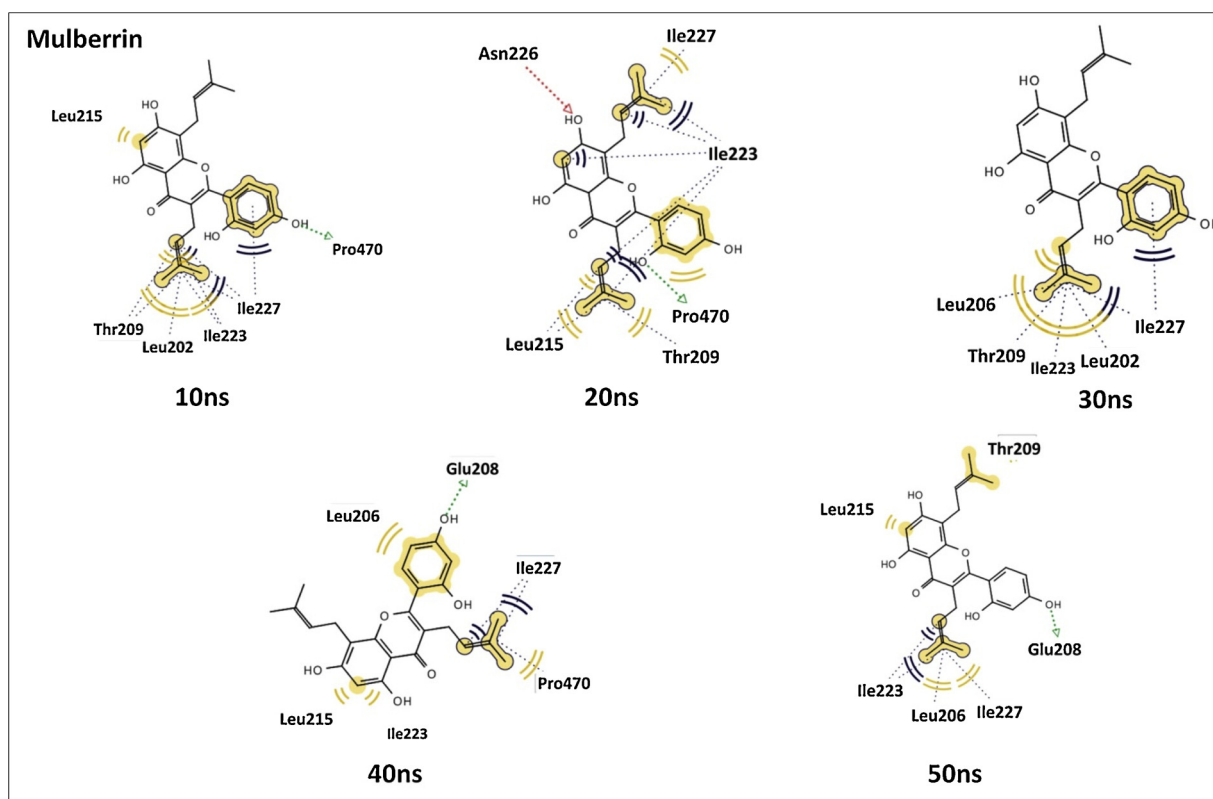


Fig. 7. The binding site for the residues of SIRT1 [4ZZJ:NAD⁺:Zn:peptide] complex with the mulberrin of the trajectory at the end of 50 frames of 10, 20, 30, 40, and 50 ns simulation.

Gartanin-SIRT1 complex show interaction of methyl butenyl group with Ile223 and methyl butenyl, benzene of xanthone group with Ile227 at the allosteric site of the trajectory at the end of 50 frames of 10, 20, 30, 40, and 50 ns simulation (Table 2, Supplementary Fig. 11). Gartanin with the SIRT1 showed the minimum binding free energy (MM-GBSA $\Delta G = -24.9 \pm 2.578$ kcal/mol) at 30 ns, with interactions of methyl butenyl group with Leu202, Thr209, Leu215, Ile223, Ile227. The maximum binding free energy at 40 ns show the interactions with Leu206, Leu215, Ile223, Ile227 as HI, and Glu230 [OH-O] as HBD; The difference between the maximum and minimum energy $\Delta = 7.97$ kcal/mol. The minimum binding free energy MM-PBSA ΔG was -22.383 kcal/mol, at 30 ns; the difference with the maximum energy, at 40 ns, was $\Delta = 4.224$ kcal/mol.

Nicotinamide as SIRT1 inhibitor was docked into the allosteric region of SIRT1 for MD simulation resulting MM-GBSA $\Delta G = -4.456 \pm 1.072$ kcal/mol at 10 ns, showed hydrophobic interactions of the pyridine of nicotinamide with Leu202, Leu206, Ile223. Then, at 20 ns of MD simulation there was no interaction observed between nicotinamide with SIRT1 at allosteric region. Nicotinamide is known as SIRT1 inhibitor, and it was proven that no interaction between nicotinamide with SIRT1 at allosteric region, after 10 ns.

These findings showed that mulberrin, quinine, quinidine, and gartanin compounds had different energy values for MM-GBSA and MM-PBSA of the trajectory at the end of 50 frames of 10, 20, 30, 40, and 50 ns simulation, in the range values 0.328–4.726 kcal/mol, within the standard error of the MMGB(PB)SA binding free energy. The interaction of mulberrin, quinine, quinidine, and gartanin with SIRT1 showed the activation of sirtuin that indicated by SIRT1 activator interactions in the allosteric region [α H2 and α H3], in accordance with the known mechanism for SIRT1 activation (Dai et al., 2010).

3.6. In vitro assays of the candidate SIRT1 activators

The in vitro study (SIRT-Glo™) assays and SIRT-Glo™ enzyme of mulberrin, quinine, quinidine, gartanin were performed in duplicate, using serial dilution to obtain concentrations of 220 μ M. Based on the results of determining linear range using SIRT-Glo™ enzymes (Supplementary Fig. 12). Thus, the concentration of the enzyme used was 0.125 μ M within the linear range determined for activators or inhibitors, because, the enzyme concentration of 1.5 μ g/mL, 2.0 μ g/ml and 2.5 μ g/ml had the same luminescence (RLU) value (6×10^6). Activator profiles for SIRT1-Glo™ obtained from the assays of mulberrin, quinine, quinidine, and gartanin, showing the relationship between the concentrations of 55, 27.5, 13.75, 6.875, 3.44, and 1.7 μ M of each compound and the % activation of SIRT1 (Fig. 8).

The compound mulberrin, quinine, quinidine, and gartanin has been identified as SIRT1 activator with EC_{50} values were 2.10 ± 0.285 , 1.14 ± 0.067 , 1.71 ± 0.035 , and 1.79 ± 0.095 μ M, respectively. In comparison, nicotinamide as SIRT inhibitor controls showed $IC_{50} = 87.59$ μ M, profile (Supplementary Fig. 13). Resveratrol (SIRT1 activator) has been reported to have an EC_{50} of 23.6 μ M (Wu et al., 2013) or 46.2 μ M (Hubbard and Sinclair, 2014). Results proved that mulberrin, quinine, quinidine, and gartanin are a significant activator of SIRT1 activity as evident from the results of activation assay.

3.7. In silico and in vitro correlation

Correlations were calculated between the in vitro SIRT1 activation EC_{50} values for mulberrin (2.10 μ M), quinine (1.14 μ M), quinidine (1.71 μ M), and gartanin (1.79 μ M), (Fig. 8, with their in silico molecular docking bond energies (ΔG) and with the MM-PB(GB)SA binding free energy (ΔG) in the MD simulation of trajectory conformation at the end of 50 frames of 10, 20, 30, 40, 50 ns (Table 2, Supplementary Fig. 11). The correlation between the EC_{50} and the molecular docking score values was $R^2 = 0.1303$. Thus, the molecular docking bonding free energy for the four compounds showed no correlation with the

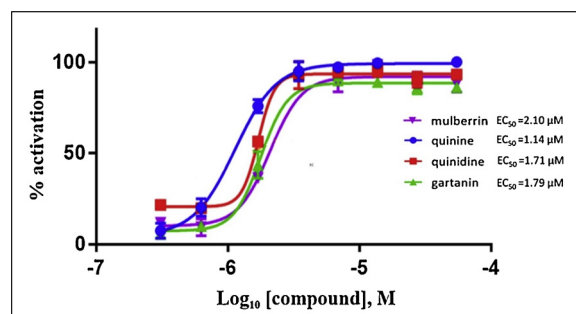


Fig. 8. Activator profiles for SIRT1-Glo™ obtained from the assays of mulberrin, quinine, quinidine, and gartanin, showing the relationship between the concentration of each compound and the % activation of SIRT1.

biological in vitro data. The correlation between the EC_{50} and ΔG MM-GBSA values were as follows: 10 ns, $R^2 = 0.867$; 40 ns, $R^2 = 0.923$; and 50 ns, $R^2 = 0.919$. The correlation between EC_{50} and ΔG MM-PBSA values were as follows: 20 ns, $R^2 = 0.828$; 40 ns, $R^2 = 0.942$; and 50 ns, $R^2 = 0.928$.

Thus, the performance of MM-GBSA binding free energy (ΔG) at 10, 40, and 50 ns and MM-PBSA binding free energy at 20, 40, and 50 ns, results for the [4ZZJ:NAD⁺:Zn:peptide] complex with mulberrin, quinine, quinidine, and gartanin showed significant correlations to the in vitro results. Karaman et al. (Karaman and Sippl, 2015) reported a correlation between MM-GBSA binding affinity and in vitro value of $R^2 = 0.75$ for inhibitor:SIRT1 complex. The interaction among the ligand and [4ZZJ:NAD⁺:Zn:peptide] receptor provides evidence that mulberrin, quinine, quinidine gartanin acts as a SIRT1 activator (Dai et al., 2015).

4. Conclusions

Pharmacophore-based virtual screening using structure-based pharmacophores predicted that mulberrin, with four hydrophobic interactions and one hydrogen bond as a HBA, was the best candidate SIRT1 activator. Pharmacophore-based virtual screening using ligand-based pharmacophores predicted that quinine, quinidine, and gartanin compounds, with two hydrophobic interactions, two aromatic rings, and one HBA, were the best candidate SIRT1 activators. Molecular docking studies of mulberrin, quinine, quinidine, gartanin with 4ZZJ, showed the important residues involved in hydrophobic interactions (HI) were Ile223 and Ile227. In the in vitro studies, the EC_{50} values of mulberrin, quinine, quinidine, and gartanin were 2.1, 1.14, 1.71, and 1.79 μ M, respectively, which were within the range of concentrations needed to activate SIRT1. Thus, mulberrin, quinine, quinidine, and gartanin are predicted to be candidate SIRT1 activators. The analysis of the correlation between the in silico and in vitro results for mulberrin, quinine, quinidine, and gartanin using MM/PB(GB)SA predicted they had good activity as SIRT1 activators.

Funding

This work was supported by the PITTA 2018 under contract number 1763/UN2.R3.1/HKP.05.00/2018 to AY from Universitas Indonesia.

Declaration of Competing Interest

None.

Acknowledgements

We thank Prof. Dr. Muhammad Hanafi, Indonesia Institute of Science (LIPI), Research Center of Chemistry.

Appendix A. Supplementary data

Supplementary data associated with this article can be found, in the online version, at <https://doi.org/10.1016/j.compbiolchem.2019.107096>.

References

- Bendix, F., Wolber, G., Seidel, T., 2010. Strategies for 3D pharmacophore-based virtual screening. *Drug Discov. Today Technol.* 7, e221–e228.
- Bruckbauer, A., Zemel, M.B., 2013. Synergistic effects of metformin, resveratrol, and hydroxymethylbutyrate on insulin sensitivity. *Diabetes Metab. Syndr. Obes. Targets Ther.* 6, 93–102. <https://doi.org/10.2147/DMSO.S40840>.
- Case, D.A., Darden, T., III, T.E.C., Simmerling, C., Brook, S., Roitberg, A., et al., 2014. Amber 14. Ref Man [Internet]. Available from: <http://ambermd.org/contributors>.
- Dai, H., Case, A.W., Riera, T.V., Considine, T., Lee, J.E., Hamuro, Y., Zhao, H., Jiang, Y., Sweitzer, S.M., Pietrak, B., Schwartz, B., Blum, C.A., Disch, J.S., Caldwell, R., Szczepankiewicz, B., Oalman, C., Yee Ng, P., White, B.H., Casabon, R., Narayan, R., Koppetsch, K., Bourbonais, F., Wu, B., Wang, J., Qian, D., Jiang, F., Mao, C., Wang, M., Hu, E., Wu, J.C., Pemi, R.B., Vlasuk, G.P., Ellis, J.L., 2015. Crystallographic structure of a small molecule SIRT1 activator-enzyme complex. *Nat. Commun.* 6, 7645. <https://doi.org/10.1038/ncomms8645>.
- Dai, H., Kustigian, L., Carney, D., Case, A., Considine, T., Hubbard, B.P., Pemi, R.B., Riera, T.V., Szczepankiewicz, B., Vlasuk, G.P., Stein, R.L., 2010. SIRT1 activation by small molecules: kinetic and biophysical evidence for direct interaction of enzyme and activator. *J. Biol. Chem.* 285, 32695–32703. <https://doi.org/10.1074/jbc.M110.133892>.
- Dai, H., Sinclair, D.A., Ellis, J.L., Steegborn, C., 2018. Sirtuin activators and inhibitors: promises, achievements, and challenges. *Pharmacol. Ther.* 188, 140–154. <https://doi.org/10.1016/j.pharmthera.2018.03.004>.
- Genheden, S., Ryde, U., 2015. The MM/PBSA and MM/GBSA methods to estimate ligand-binding affinities. *Expert Opin. Drug Discov.* 10, 449–461. <https://doi.org/10.1517/17460441.2015.1032936>.
- Hayes, J.M., Archontis, G., 2011. MM-GB(PB)SA calculations of protein-ligand binding free energies. *Molecular Dynamics—Studies of Synthetic and Biological Macromolecules*. pp. 171–190.
- Hubbard, B.P., Sinclair, D.A., 2014. Small molecule SIRT1 activators for the treatment of aging and age-related diseases. *Trends Pharmacol. Sci.* 35, 146–154. <https://doi.org/10.1016/j.tips.2013.12.004>.
- Huynh, F.K., Hershberger, K.A., Hirschev, M.D., 2013. Targeting sirtuins for the treatment of diabetes. *Diabetes Manag. (Lond.)* 3, 245–257. <https://doi.org/10.2217/dmt.13.6>.
- Karaman, B., Sippl, W., 2015. Docking and binding free energy calculations of sirtuin inhibitors. *Eur. J. Med. Chem.* 93, 584–598. <https://doi.org/10.1016/j.ejmech.2015.02.045>.
- Kästner, J., Loeffler, H.H., Roberts, S.K., Martin-Fernandez, M.L., Winn, M.D., 2009. Ectodomain orientation, conformational plasticity and oligomerization of ErbB1 receptors investigated by molecular dynamics. *J. Struct. Biol.* 167, 117–128. <https://doi.org/10.1016/j.jsb.2009.04.007>.
- Kitada, M., Koya, D., 2013. SIRT1 in Type 2 diabetes: mechanisms and therapeutic potential. *Diabetes Metab. J.* 37, 315–325. <https://doi.org/10.4093/dmj.2013.37.5.315>.
- Kitada, M., Ogura, Y., Koya, D., 2016. The protective role of Sirt1 in vascular tissue: its relationship to vascular aging and atherosclerosis. *Aging (Albany N. Y.)* 8, 2290–2307. <https://doi.org/10.18632/aging.101068>.
- Kumar, A., Chauhan, S., 2016. How much successful are the medicinal chemists in modulation of SIRT1: a critical review. *Eur. J. Med. Chem.* 119, 45–69. <https://doi.org/10.1016/j.ejmech.2016.04.063>.
- Lee, M.C., Duan, Y., 2004. Distinguish protein decoys by using a scoring function based on a new AMBER force field, short molecular dynamics simulations, and the generalized born solvent model. *Proteins* 55, 620–634. <https://doi.org/10.1002/prot.10470>.
- Lipinski, C.A., 2004. Lead- and drug-like compounds: the rule-of-five revolution. *Drug Discov. Today Technol.* 1, 337–341. <https://doi.org/10.1016/j.ddtec.2004.11.007>.
- Liu, Q., Chen, L., Hu, L., Guo, Y., Shen, X., 2010. Small molecules from natural sources, targeting signaling pathways in diabetes. *Biochim. Biophys. Acta* 1799, 854–865. <https://doi.org/10.1016/j.bbagr.2010.06.004>.
- Mellini, P., Valente, S., Mai, A., 2015. Sirtuin modulators: an updated patent review (2012–2014). *Expert Opin. Ther. Patents* 25, 5–15. <https://doi.org/10.1517/13543776.2014.982532>.
- Miller, B.R., Mcgee, T.D., Swails, J.M., Homeyer, N., Gohlke, H., Roitberg, A.E., 2012. MMPBSA.py: an efficient program for end-state free energy calculations. *Am. Chem. Soc.* 8, 3314–3321.
- Mysinger, M.M., Carchia, M., Irwin, J.J., Shoichet, B.K., 2012. Directory of useful decoys, enhanced (DUD-E): better ligands and decoys for better benchmarking. *J. Med. Chem.* 55, 6582–6594. <https://doi.org/10.1021/jm300687e>.
- Nakagawa, T., Guarente, L., 2011. Sirtuins at a glance. *J. Cell. Sci.* 124, 833–838. <https://doi.org/10.1242/jcs.081067>.
- Ogetii, G.N., Akech, S., Jemutai, J., Boga, M., Kivaya, E., Fegan, G., Maitland, K., 2010. Hypoglycaemia in severe malaria, clinical associations and relationship to quinine dosage. *BMC Infect. Dis.* 10, 334. <https://doi.org/10.1186/1471-2334-10-334>.
- Pavelites, J.J., Gao, J., Bash, Pa., 1996. A molecular mechanics force field for NAD⁺, NADH, and the pyrophosphate groups of nucleotides. *J. Comput. Chem.* 18, 221–239.
- Pedraza-chaverri, J., Cárdenas-rodríguez, N., Orozco-ibarra, M., Pérez-rojas, J.M., 2008. Medicinal properties of mangosteen (*Garcinia mangostana*). *Food Chem. Toxicol.* 46 (10), 3227–3239.
- Phillips, R.E., Looareesuwan, S., White, N.J., Chanthavanich, P., Karbwang, J., Supanaranond, W., Turner, R.C., Warrell, D.A., 1986. Research from the South Hypoglycaemia and antimalarial drugs: quinidine and release of insulin. *Br. Med. J. (Clin. Res. Ed.)* 292, 1319–1321.
- Pulla, V.K., Alvala, M., Sriram, D.S., Viswanadha, S., Sriram, D., Yogeewari, P., 2014. Structure-based drug design of small molecule SIRT1 modulators to treat cancer and metabolic disorders. *J. Mol. Graph. Model.* 52, 46–56. <https://doi.org/10.1016/j.jmgm.2014.06.005>.
- Pulla, V.K., Battu, M.B., Alvala, M., Sriram, D., Yogeewari, P., 2012. Can targeting SIRT-1 to treat type 2 diabetes be a good strategy? A review. *Expert Opin. Ther. Targets* 16, 819–832. <https://doi.org/10.1517/14728222.2012.703656>.
- Rodgers, J.T., Lerin, C., Haas, W., Gygi, S.P., Spiegelman, B.M., Puigserver, P., 2005. Nutrient control of glucose homeostasis through a complex of PGC-1 α and SIRT1. *Nature* 434, 113–118. <https://doi.org/10.1038/nature03354>.
- Sinclair, D., Guarente, L., 2014. Small-molecule allosteric activators of sirtuins. *Annu. Rev. Pharmacol. Toxicol.* 54, 363–380. <https://doi.org/10.1146/annurev-pharmtox-010611-134657>.
- Taber, M., Muhammad, T., Syafiq, F., Zakaria, T., Susanti, D., Zakaria, Z.A., 2016. Hypoglycaemic activity of ethanolic extract of *Garcinia mangostana* Linn. n normoglycaemic and streptozotocin- induced diabetic rats. *BMC Complement Altern Med* [Internet]. *BMC Complement. Altern. Med.* 16, 1–12. <https://doi.org/10.1186/s12906-016-1118-9>.
- Vu, Chi B., Disch, J.S., Springer, S.K., Blum, C.A., Pemi, R.B., 2014. Quinolines and Related Analogs as Sirtuin Modulators. US8685970B2. 2014. .
- Walker, R.C., De Souza, M.M., Mercer, I.P., Gould, I.R., Klug, D.R., 2002. Large and fast relaxations inside a protein: calculation and measurement of reorganization energies in alcohol dehydrogenase. *J. Phys. Chem. B* 106, 11658–11665.
- Wang, J., Wolf, R.M., Caldwell, J.W., Kollman, P.A., Case, D.A., 2004. Development and testing of a general amber force field. *J. Comput. Chem.* 25, 1157–1174. <https://doi.org/10.1002/jcc.20035>.
- Wang, A., Li, D., Wang, S., Zhou, F., Li, P., Wang, Y., Lin, L., 2018. γ -Mangostin, a xanthone from mangosteen, attenuates oxidative injury in liver via NRF2 and SIRT1 induction. *J. Funct. Foods* 40 (November 2017), 544–553.
- Wanga, X., Fan Yia, N., 2012. Histone deacetylases and their inhibitors: molecular mechanisms and therapeutic implications in diabetes mellitus. *Acta Pharm. Sin. B* 2, 387–395. <https://doi.org/10.1016/j.apsb.2012.06.005>.
- Wilson, R.D., Islam, S., 2015. Effects of white mulberry (*Morus alba*) leaf tea investigated in a type 2 diabetes model of rats. *Acta Poloniae Pharmaceutica n Drug Research* 72 (1), 153–160 2015.
- Wolber, G., Langer, T., 2005. LigandScout: 3-D pharmacophores derived from protein-bound ligands and their use as virtual screening filters. *J. Chem. Inf. Model.* 45, 160–169. <https://doi.org/10.1021/ci049885e>.
- Wu, J., Zhang, D., Chen, L., Li, J., Wang, J., Ning, C., Yu, N., Zhao, F., Chen, D., Chen, X., Chen, K., Jiang, H., Liu, H., Liu, D., 2013. Discovery and mechanism study of SIRT1 activators that promote the deacetylation of fluorophore-labeled substrate. *J. Med. Chem.* 56, 761–780. <https://doi.org/10.1021/jm301032j>.
- Yang, S.Y., 2010. Pharmacophore modeling and applications in drug discovery: challenges and recent advances. *Drug Discov. Today* 15, 444–450. <https://doi.org/10.1016/j.drudis.2010.03.013>.
- Yanuar, A., Mun'im, A., Lagho, A.B.A., Syahdi, R.R., Rahmat, M., Suhartanto, H., 2011. Medicinal plants database and three dimensional structure of the chemical compounds from medicinal plants in Indonesia. *Int. J. Comput. Sci.* 8, 180–183.